Journal of Power Sources 237 (2013) 295–299

Contents lists available at SciVerse ScienceDirect

Journal of Power Sources

journal homepage: www.elsevier.com/locate/jpowsour

Short communication

Enhanced photoelectrochemical performance of hydrogenated ZnO hierarchical nanorod arrays

Chenzhong Yao [a,*], Bohui Wei [a], Huixuan Ma [a], Hui li [a], Lixin Meng [a], Xisheng Zhang [b], Qiaojuan Gong [a,*]

[a] Department of Applied Chemsitry, Yuncheng University, Yuncheng 044000, People's Republic of China
[b] Department of Physics and Electronic Engineering, Yuncheng University, Yuncheng 044000, People's Republic of China

HIGHLIGHTS

- The preparation of hydrogenated ZnO hierarchical nanorod arrays is reported.
- Oxygen vacancies are formed in hydrogenated ZnO.
- Hydrogenated ZnO hierarchical nanorod arrays have an improved donor density and IPCE.

GRAPHICAL ABSTRACT

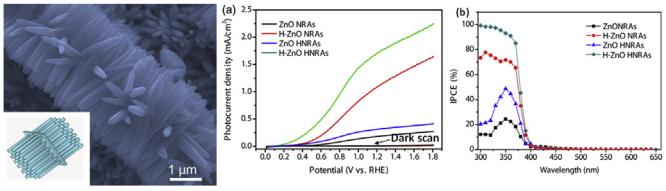

ARTICLE INFO

Article history:
Received 3 January 2013
Received in revised form
14 February 2013
Accepted 23 February 2013
Available online 15 March 2013

Keywords:
Hydrogenated
Nanorod arrays
Electrodeposition
Photo-anode

ABSTRACT

Hydrogenated ZnO (H-ZnO) hierarchical nanorod arrays (HNRAs) with enhanced photoelectrochemical performance have been reported for the first time. The H-ZnO samples were obtained by annealing the ZnO nanorod arrays (NRAs) and HNRAs in hydrogen atmosphere at 350 °C for 60 min. The electrochemical impedance measurements indicate the donor density of H-ZnO HNRAs achieved 5.1×10^{18} cm^{-3}, which is higher than those of other ZnO samples. These H-ZnO HNRAs yields an improved photocurrent density of 1.72 mA cm^{-2} at 1.23 V vs. RHE, and the incident-photon-to-current-conversion efficiency (IPCE) values uniformly higher than 90% in the wavelength range from 300 to 370 nm, which are substantially higher than the pristine ZnO NRAs, ZnO HNRAs and H-ZnO NRAs. The ability to improve the photoelectrochemical properties of ZnO electrode materials may open up new opportunities for high-performance photovoltaic cells.

1. Introduction

Increasing demand for sustainable energy and growing concern on environmental protection have motivated considerable interest to exploit and develop various solar-harvesting and conversion devices [1,2]. Photoelectrochemical water splitting over semiconductor photo-anodes is extensively regarded as a very promising approach to produce hydrogen gas by utilizing solar energy [3–5]. Various metal oxides such as TiO_2, [4] In_2O_3, [5] WO_3, [6,7] ZnO, [8,9] Fe_2O_3 [10] have been widely investigated as photoanodes for photoelectrochemical hydrogen evolution from splitting water. Among them, ZnO has been extensively used as photoanode for photoelectrochemical water splitting because of its suitable band-edge positions, low cost and environmental friendly [8,11–13]. The main drawback of ZnO as photoanode is its poor light-harvesting ability of visible light and quick recombination of photo-generated carriers, which makes its efficiency is still low at present [12–14].

Recently, one-dimensional vertical (1D) ZnO nanostructures such as nanorods (NRs), nanowires (NWs) and nanotubes (NTs) have drawn considerable interest for photoelectrochemical water splitting due to their high accessible area and efficient diffusion path of charge carriers [12,15–17]. In comparison with single 1D ZnO nanostructures, hierarchical ZnO architectures that assembled by 1D nanostructures are more attractive for photoelectrochemical splitting water because they combine the features of micrometer- and nanometer-scaled building blocks, provide higher surface area and faster charge separation and transport [9,18]. This is because

* Corresponding authors. Tel.: +86 359 8594394.
E-mail addresses: yaochzh1999@126.com (C. Yao), wei623124304@163.com (B. Wei), gqjuan@163.com (Q. Gong).

0378-7753/$ – see front matter © 2013 Elsevier B.V. All rights reserved.
http://dx.doi.org/10.1016/j.jpowsour.2013.02.062

higher surface area of hierarchical ZnO architectures can reduce the distance that charge carriers must travel, enhance the light absorption, and hence enable near-unity collection efficiencies [19]. Several approaches have been proposed to prepare hierarchical ZnO architectures, but it still remains a big challenge to develop simple and reliable synthetic methods for hierarchical architectures.

On the other hand, recent reports have demonstrated that the photoactives of metal oxides can be enhanced by hydrogenation, [4,6,20–23] and hydrogenated ZnO nanorod arrays (NRAs) for photocatalytic and photoelectrochemical hydrogen production have been reported recently [21,24]. However, to the best of our knowledge, the influence of hydrogenation on the photoelectrochemical properties of hierarchical ZnO architectures has never been studied yet. In this paper, we report a facile method for the growth of hydrogenated ZnO (denoted as H-ZnO) hierarchical nanorod arrays (HNRAs) and their enhanced photoelectrochemical properties.

2. Experimental section

2.1. Preparation of the H-ZnO nanorod arrays (NRAs) and hierarchical nanorod arrays (HNRAs)

All reagents used were analytical grade and were used directly without any purification. All the electrochemical deposition experiments were carried out in a conventional three-electrode glass cell by cathodic electrodeposition. A glass coated with F-doped SnO_2 (FTO) with a sheet resistance of 14 Ω sq^{-1} was used as the working electrode, a Pt wire (0.2 cm^2) was used as the counter electrode, and a Ag/AgCl was used as the reference electrode that connect to the cell with a double salt bridge. Prior to electrodeposition, the FTO glass was cleaned ultrasonically in distilled water, ethanol, and acetone and then rinsed in distilled water again. ZnO NRAs were directly grown on FTO substrate in a solution of 0.02 M $Zn(NO_3)_2$ and 0.01 M ammonium acetate (CH_3COONH_4) with a current density of 2.0 mA cm^{-2} at 90 °C for 30 min. ZnO HNRAs were prepared by a two-step electrochemical process [25,26]. Firstly, ZnO microsheets were grown on FTO substrate with a current density of 1.0 mA cm^{-2} for 5 min in a solution containing 0.05 M $Zn(CH_3COO)_2$. Secondly, the FTO substrate coated with ZnO microsheets served as working electrode and performed in a solution of 0.02 M $Zn(NO_3)_2$ and 0.01 M CH_3COONH_4 at 90 °C for 30 min electrodeposition under a current density of 2.0 mA cm^{-2}. All the as-prepared samples were thoroughly washed with ethanol and then distilled water, and then were annealed at 350 °C for 60 min in air to enhance the mechanical stability and electrical conductivity. Finally, hydrogenated ZnO (H-ZnO) NRAs and HNRAs were obtained by annealing the ZnO NRAs and HNRAs in hydrogen atmosphere at 350 °C for 60 min. The preparation was performed in a home-built tube furnace filled with hydrogen gas.

2.2. Structural characterization

The morphology and the microstructure of the products were characterized by mean of field emission scanning electron microscope (FE-SEM, JSM-6330F) and transmission electron microscopy (TEM, JEM2010-HR, 200 kV). The structure and composition of the samples were investigated via X-ray diffraction (XRD, Bruker, D8 ADVANCE) with Cu Kα radiation (λ = 1.5418 Å) and X-ray Photoelectron Spectroscopy (XPS, ESCALab250, Thermo VG) with 200 W Al KR radiation in twin anode. UV–Visible diffusive reflectance spectra of samples were recorded on a VARIAN CARY 5000 UV–Vis–NIR spectrophotometer.

2.3. Photoelectrochemical measurements

All the electrochemical tests were performed in a three-electrode electrochemical cell with a flat quartz glass. The working electrode area is in the range of 0.2–0.25 cm^2 and the electrolyte is 0.5 M Na_2SO_4 aqueous solution. Linear sweeps were measured by a CHI 660D electrochemical workstation, with a Pt wire (0.2 cm^2) as counter electrode and Ag/AgCl as reference electrode under simulated sunlight (100 $mWcm^{-2}$) with a 150 W xenon lamp coupled with an AM 1.5 global filter. Mott-Schottky plots were generated based on capacitances that were derived from the electrochemical impedance obtained at each potential with 10 kHz frequency in the dark. Incident-photon-to-current-conversion-efficiencies (IPCE) were collected by a CHI 660D electrochemical station with a solar simulator (Newport 69920, 500 W xenon lamp), coupled with an infrared water filter (Oriel 6127) and aligned monochromator (Oriel Cornerstone 130 1/8 m), and the wavelength scanning ranges between 300 and 650 nm.

3. Results and discussion

3.1. Morphology of hydrogenated ZnO hierarchical nanorod arrays

Firstly, ZnO microsheets was grown on FTO substrate by cathodic deposition as shown in Fig. 1a. And then, the ZnO HNRAs were obtained through sequential electrodeposition on the FTO substrate coated with ZnO microsheets. Free-standing ZnO nanorods annealed in air (Fig. 1b–c) were successfully grown on the both sides of microsheets. These ZnO nanorods have a diameter of 200–300 nm and a length of about 1.7 μm. Hierarchical H-ZnO architectures were obtained by hydrogenation treatment of the sample in a home-built tube furnace system that filled with hydrogen gas at 350 °C for 60 min. As shown in Fig. 1d, the morphology of these hierarchical architectures did not changed during the hydrogenation. Transmission electron microscopy (TEM) and selected area electron diffraction (SAED) analyzes (Fig. 1e) show that the H-ZnO nanorod is single crystalline with a growth direction of [001]. High resolution transmission electron microscopy (HRTEM) image in Fig. 1f displays a well-resolved lattice fringes of 0.52 nm, corresponding to the (001) plane of wurtzite ZnO (JCPDF # 36-1451), which further confirms the single crystallinity of H-ZnO nanorod. It should be noted that only ZnO nanorod arrays were obtained on FTO substrate without the microsheets layer (Fig. 2), which confirms the pre-formed microsheets play an important role in forming the hierarchical ZnO architecture.

3.2. Structure, UV–vis spectra and electrical properties

To detect the possible phase change during hydrogenation, we performed X-ray diffraction (XRD) studies. XRD patterns collected from pristine ZnO and H-ZnO samples (Fig. 3) show that their diffraction peaks can be indexed to hexagonal wurtzite structure of ZnO (JCPDF# 36-1451). However, the H-ZnO sample shows broader and weaker peaks compared to pristine ZnO sample, disclosing some defects are introduced to ZnO NRs during hydrogenation.

The color of the white ZnO film changed to black after hydrogenation (the inset of Fig. 4a, which is in agreement with the phenomenon observed by Lu et al. [20]. To investigate the influence of hydrogenation on the optical property of ZnO, diffuse reflectance UV–vis spectra collected formed ZnO samples and H-ZnO samples are shown in Fig. 4a. The low reflectance for both the samples in the UV region is mainly attributed to their strong UV light-harvesting ability. In comparison to the ZnO sample, H-ZnO sample shows much lower reflectance in the range of 400–650 nm, which suggests that H-ZnO sample may utilize visible light much better. This

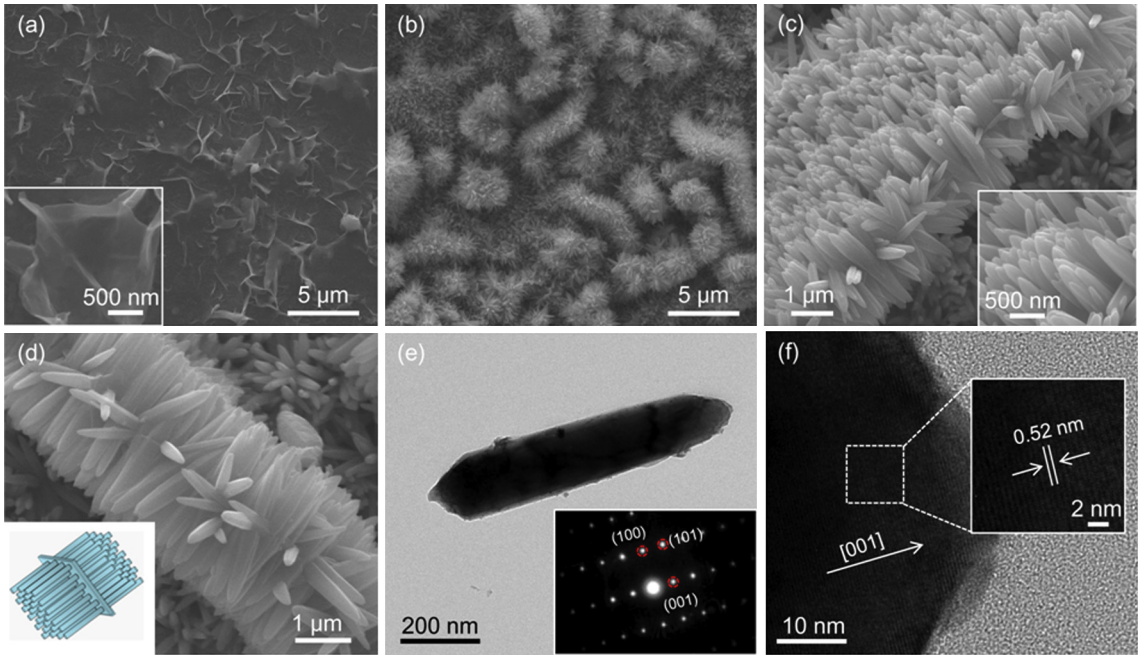

Fig. 1. (a) SEM images of as-prepared ZnO microsheets. (b–c) SEM images of the ZnO HNRAs by using the ZnO microsheets as a template. (c) SEM image of H-ZnO HNRAs. Inset is a schematic diagram of H-ZnO HNRAs. (e) TEM image of single H-ZnO nanorod from H-ZnO HNRAs. Inset is the SAED pattern that recorded from the H-ZnO NR. (f) HRTEM images of the H-ZnO nanorod.

enhanced visible light absorption of H-ZnO NRAs is due to the formation of impurity/defect states in the band gap of ZnO during hydrogen treatment [21].

To further investigate the defects of the H-ZnO sample, X-ray photoelectron spectroscopy (XPS) analyzes were also performed. Fig. 4b shows the normalized Zn 2p core level XPS spectra of ZnO and H-ZnO HNRAs. Both the samples exhibit two peaks at about 1021 and 1044.1 eV, which are the characteristic Zn $2p_{3/2}$ and Zn $2p_{1/2}$ peaks of ZnO [27]. Fig. 4c compares the normalized O 1s core level XPS spectra of ZnO and H-ZnO samples. Two peaks located at 529.9 eV and 531.5 eV are clearly identified in both the ZnO and H-ZnO samples. The peak at 529.9 eV is attributed to the characteristic peak of Zn–O–Zn, while the peaks centered at 531.5 eV are ascribed to Zn-OH [27]. Compared to the ZnO sample, the Zn-OH peak intensity of H-ZnO sample is much stronger, indicating the H-ZnO sample has more hydroxyl groups and oxygen vacancies [20,21].

To study the effect of hydrogenation on the electrical properties of ZnO HNRAs, we performed electrochemical impedance measurements in the dark with 0.5 M Na_2SO_4 as electrolyte. For better comparison, ZnO NRAs, H-ZnO NRAs and ZnO HNRAs photoelectrodes were also tested in the same conductions. Fig. 4d shows the Mott-Schottky plots of the ZnO NRAs, H-ZnO NRAs, ZnO HNRAs and H-ZnO HNRAs, which were generated based on capacitances that were derived from the electrochemical impedance obtained at each potential with 10 kHz frequency in the dark. As expected for *n*-type semiconductor, both the ZnO and ZnO HNRAs exhibit positive slopes in the Mott-Schottky plots. As expected, the H-ZnO samples show relatively smaller slopes compared to ZnO sample, suggesting the increased donor densities (carrier densities) after hydrogen treatment according to the Mott-Schottky equation: [28]

$$N_d = (2/e_0\varepsilon\varepsilon_0)\left[\mathrm{d}\left(1/C^2\right)/\mathrm{d}V\right]^{-1}$$

where N_d is the donor density, e_0 the electron charge, ε the dielectric constant of ZnO ($\varepsilon = 8$), [29] ε_0 the permittivity of vacuum, and V the applied bias at the electrode. The carrier densities of the ZnO NRAs, ZnO HNRAs, H-ZnO NRAs and H-ZnO HNRAs are calculated to be 2.4×10^{18} cm^{-3}, 3.3×10^{18} cm^{-3}, 3.1×10^{19} cm^{-3}

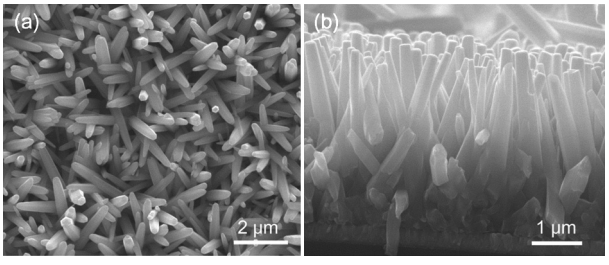

Fig. 2. SEM images of the ZnO NRAs obtained with a current density of 2.0 mA cm^{-2} for 60 min in a solution 0.02 M $Zn(NO_3)_2$ and 0.01 M CH_3COONH_4 at 90 °C.

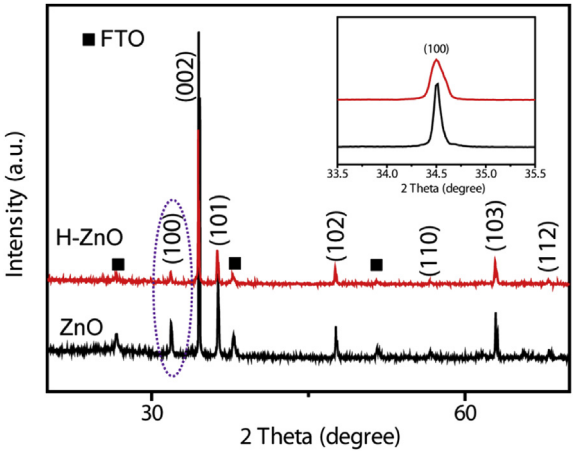

Fig. 3. XRD spectra collected for ZnO and H-ZnO HNRAs. Inset is the magnified view of the XRD spectra of the (100) peak.

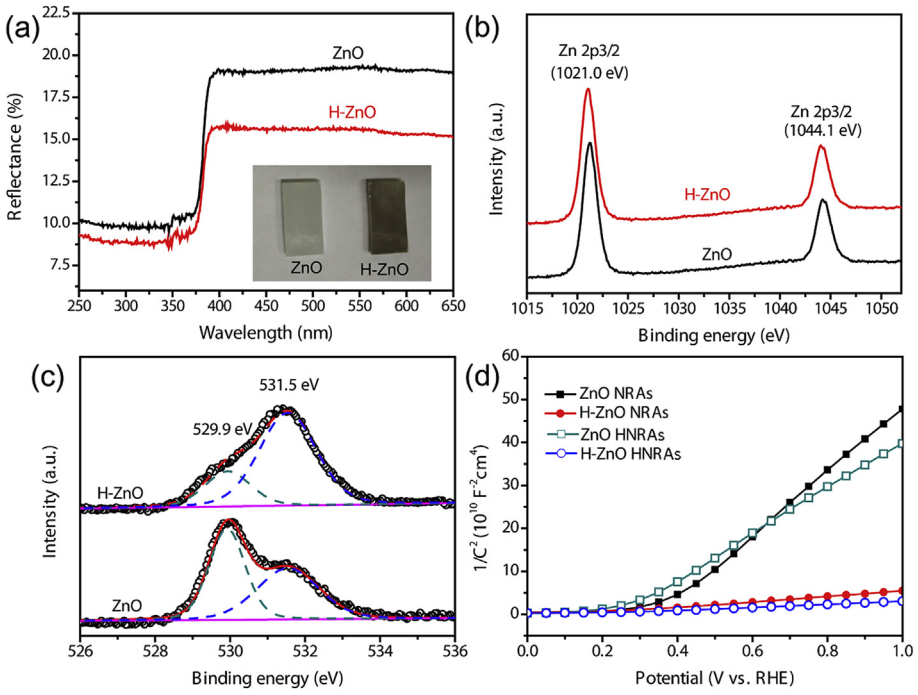

Fig. 4. (a) Diffuse reflectance UV–visible spectra of ZnO and H-ZnO HNRAs. Inset is the picture of ZnO and H-ZnO HNR films. (b) Zn 2p and (c) O1s core level XPS spectra of ZnO and H-ZnO HNRAs. (d) Mott-Schottky plots collected from ZnO NRAs, H-ZnO NRAs, ZnO HNRAs and H-ZnO HNRAs at a frequency of 10 kHz in the dark.

and 5.1×10^{19} cm^{-3}, respectively. It should be pointed out that Mott-Schottky equation is derived based on planar structure and it may not able to determine precisely the donor density of nanostructured materials. However, given that the ZnO and H-ZnO samples have similar morphology, a qualitative comparison of carrier densities between them is reasonable. Obviously, the H-ZnO samples exhibit much higher carrier density (more than 10-fold enhancement) than that of other ZnO samples. The present values are also higher than that of recently reported ZnO NRAs (only 4-fold enhancement after hydrogenation). The increased carrier density of the H-ZnO samples can be attributed to the increased oxygen vacancies and hydrogen impurities [4]. The hydrogen impurities in ZnO during hydrogenation are easily formed and have been reported [30,31]. However, due to the lack of instruments, we were not able to determine the presence of hydrogen impurities.

3.3. Photoelectrochemical performance

To evaluate the photoelectrochemical property of these H-ZnO HNRAs, photoelectrochemical measurements were conducted in a three-electrode electrochemical cell with a Pt wire as counter electrode and an Ag/AgCl as reference electrode in 0.5 M Na_2SO_4 solution. Fig. 5a compares the photocurrent responses of ZnO NRAs, H-ZnO NRAs, ZnO HNRAs and H-ZnO HNRAs recorded with simulated sunlight illumination at 100 $mWcm^{-2}$ (AM 1.5G). The potential was measured against an Ag/AgCl reference and converted to reversible hydrogen electrode (RHE) potential by using the equation: $E(\mathrm{RHE}) = E(\mathrm{Ag/AgCl}) + 0.1976\mathrm{V} + 0.059\ \mathrm{pH}$. Dark scan linear sweep voltammograms from 0 to +1.8 V (vs. RHE) showed a small current in the range of 10^{-4} mA cm^{-2}. The as-prepared ZnO NRAs and ZnO HRNAs yielded relatively low photocurrent densities of 0.18 mA cm^{-2} and 0.31 mA cm^{-2} at 1.23 V (vs. RHE). Significantly, the photocurrent densities of the ZnO NRAs and ZnO HRNAs nanowires drastically increased after hydrogenation, which achieves 1.1 mA cm^{-2} for H-ZnO NRAs and 1.72 mA cm^{-2} for H-ZnO HNRAs at 1.23 V (vs. RHE). We examine their photocurrent response under visible light irradiation by using a UV/IR cut filer ($\lambda \geq 420$ nm). No obvious photocurrent was observed, suggesting the visible light has negligible contribution to their total photocurrent. Therefore, the enhanced photocurrent of H-ZnO NRAs and H-ZnO HNRAs may be attributed to the increased donor density, which improves the charge transport in ZnO NRAs as well as the electron transfer at the interface between the ZnO and the solution. Additionally, the HNRAs show substantially higher photocurrent densities than the NRAs, confirming these HNRAs are more promising as photoanodes for photoelectrochemical water splitting. The superior performance of the HNRAs could be attributed to their higher donor density and larger accessible surface area.

In order to address the effect of hydrogenation on light absorption of ZnO NRAs, we performed incident-photon-to-current-conversion efficiency (IPCE) measurement to characterize the photocurrent response of the photoanodes. IPCE measurements were performed on pristine ZnO and H-ZnO samples at +1.0 V vs. RHE (Fig. 5b). IPCE is expressed as $\mathrm{IPCE\%} = (1240 I_{sc})/(\lambda P_{light})$, where I_{sc} is the short-circuit photocurrent density, λ the incident light wavelength, and P_{light} is the incident light power density. Both the pristine ZnO NRAs and ZnO HNRAs exhibit low IPCE values in UV region. In contrast, the H-ZnO NRAs and H-ZnO HNRAs exhibit significantly enhanced photoactivity over the entire UV region, suggesting the utilization of the UV light is more efficient after hydrogenation. For example, the IPCE value of H-ZnO NRAs collected at the incident wavelength of 350 nm achieves about 71%, while only about 26% for the pristine ZnO NRAs. This clearly indicates the hydrogenation can greatly improve the photoelectrochemical property of ZnO. The H-ZnO HNRAs has the largest IPCE values that uniformly higher than 90% in the wavelength range from 300 to 370 nm, which indicates that the UV light was effectively used for PEC water splitting, and the separation and transportation of photoexcited charge carriers are very efficient in the H-ZnO sample. In addition, no visible light photoactivities were observed for all the samples. All these findings again confirm that

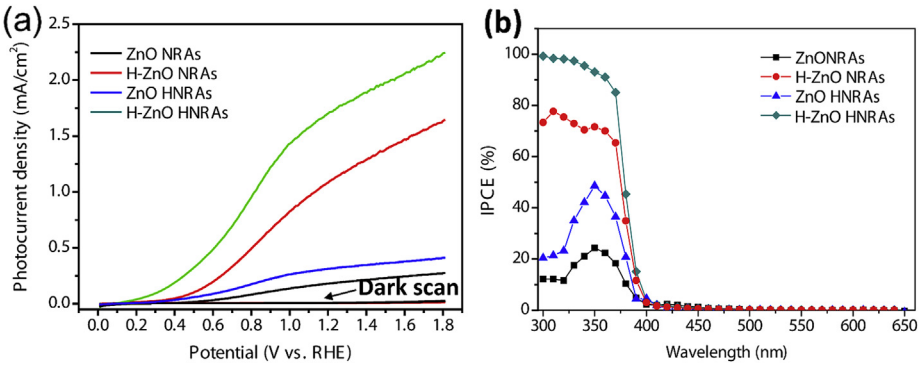

Fig. 5. (a) Linear sweeps voltammogram and (b) measured IPCE spectra collected at the incident wavelength range from 300 to 650 nm at a potential of +1.0 V vs. RHE.

the enhanced photocurrent in H-ZnO samples is mainly attributed to the improved UV light utilization and enhanced donor density.

4. Conclusions

In summary, we have demonstrated a facile electrochemical method to prepare hierarchical ZnO NRAs and hydrogen treatment is an effective method to improve the photoelectrochemical property of ZnO nanostructures. The H-ZnO samples were obtained by annealing the ZnO NRAs and HNRAs in hydrogen atmosphere at 350 °C for 60 min. The H-ZnO HNRAs exhibits strong light absorption in UV region, and thereby the carrier density. The photocurrent and IPCE of H-ZnO HNRAs were enhanced compared to the pristine ZnO NRAs, ZnO HNRAs and H-ZnO NRAs in electrolyte. More importantly, this present strategy to prepare the highly photoactive H-ZnO HNRAs may open up new opportunities for their applications in other fields, such as dye-sensitized solar cells, and photocatalysis.

Acknowledgments

This work was supported by the Natural Science Foundations of China (Grant Nos. J1103305, 51101138 and 90923008), the Natural Science Foundation of Shanxi Province (Grant No. 2012021020-3 and 2012011007-1), the S & T Project of Shanxi Province (Grant No. 20111024), the Excellent Young Academic Leaders Project of Colleges and Universities of Shanxi, the State Key Laboratory of Solidification Project (Grant No. SKLSP201227), and Young Teacher Starting-up Research of Yuncheng University. We also thank X.H. Lu and T. Zhai (Sun Yat-sen University) for the help of IPCE measurements.

References

[1] J.Z. Su, X.J. Feng, J.D. Sloppy, L.J. Guo, C.A. Grimes, Nano Lett. 11 (2011) 203–208.
[2] C.Z. Yao, B.H. Wei, L.X. Meng, H. Li, Q.J. Gong, H. Sun, H.X. Ma, X.H. Hu, J. Power Sources 207 (2012) 222–228.
[3] X.H. Lu, D.Z. Zheng, P. Zhang, C.L. Liang, P. Liu, Y.X. Tong, Chem. Commun. 46 (2010) 7721–7723.
[4] G.M. Wang, H.Y. Wang, Y.C. Ling, Y.C. Tang, X.Y. Yang, R.C. Fitzmorris, C.C. Wang, J.Z. Zhang, Y. Li, Nano Lett. 11 (2011) 3026–3033.
[5] J.Y. Gan, X.H. Lu, T. Zhai, Y.F. Zhao, S.L. Xie, Y.C. Mao, Y.L. Zhang, Y.Y. Yang, Y.X. Tong, J. Mater. Chem. 21 (2011) 14685–14692.
[6] G.M. Wang, Y.C. Ling, H.Y. Wang, X.Y. Yang, C.C. Wang, J.Z. Zhang, Y. Li, Energy Environ. Sci. 5 (2012) 6180–6187.
[7] X.H. Zhang, X.H. Lu, Y.Q. Shen, J.B. Han, L.Y. Yuan, L. Gong, Z. Xu, X.D. Bai, M. Wei, Y.X. Tong, Y.H. Gao, J. Chen, J. Zhou, Z.L. Wang, Chem. Commun. 47 (2011) 5804–5806.
[8] S.L. Xie, X.H. Lu, T. Zhai, W. Li, M.H. Yu, C.L. Liang, Y.X. Tong, J. Mater. Chem. 22 (2012) 14272–14275.
[9] Y.C. Qiu, K.Y. Yan, H. Deng, S.H. Yang, Nano Lett. 12 (2012) 407–413.
[10] Y.C. Ling, G.M. Wang, J. Reddy, C.C. Wang, J.Z. Zhang, Y. Li, Angew. Chem. Int. Ed. 51 (2012) 4074–4079.
[11] X.H. Lu, D. Wang, G.R. Li, C.Y. Su, D.B. Kuang, Y.X. Tong, J. Phys. Chem. C 113 (2009) 13574–13582.
[12] C.Y. Lin, Y.H. Lai, H.W. Chen, J.G. Chen, C.W. Kung, R. Vittal, K.C. Ho, Energy Environ. Sci. 4 (2011) 3448–3455.
[13] Y.F. Wei, L. Ke, J.H. Kong, H. Liu, Z.H. Jiao, X.H. Lu, H.J. Du, X.W. Sun, Nanotechnology 23 (2012) 235401.
[14] Y. Tak, S.J. Hong, J.S. Lee, K. Yong, J. Mater. Chem. 19 (2009) 5945–5951.
[15] X.Y. Yang, A. Wolcott, G.M. Wang, A. Sobo, R.C. Fitzmorris, F. Qian, J.Z. Zhang, Y. Li, Nano Lett. 9 (2009) 2331–2336.
[16] X.P. Qi, G.W. She, Y.Y. Liu, L.X. Mu, W.S. Shi, Chem. Commun. 48 (2012) 242–244.
[17] X.H. Zhao, P. Wang, B.J. Li, Chem. Commun. 46 (2010) 6768–6770.
[18] D.M. Tang, G. Liu, F. Li, J. Tan, C. Liu, G.Q. Lu, H.M. Cheng, J. Phys. Chem. C 113 (2009) 11035–11040.
[19] M.G. Walter, E.L. Warren, J.R. McKone, S.W. Boettcher, Q. Mi, E.A. Santori, N.S. Lewis, Chem. Rev. 110 (2010) 6446–6473.
[20] X.B. Chen, L. Liu, P.Y. Yu, S.S. Mao, Science 331 (2011) 746–750.
[21] X.H. Lu, G.M. Wang, S.L. Xie, J.Y. Shi, W. Li, Y.X. Tong, Y. Li, Chem. Commun. 48 (2012) 7717–7719.
[22] X.H. Lu, M.H. Yu, G.M. Wang, T. Zhai, S.L. Xie, Y.C. Ling, Y.X. Tong, Y. Li, Adv. Mater. 25 (2013) 267–272.
[23] X.H. Lu, G.M. Wang, T. Zhai, M.H. Yu, J.Y. Gan, Y.X. Tong, Y. Li, Nano Lett. 12 (2012) 1690–1696.
[24] J.K. Cooper, Y.C. Ling, C. Longo, Y. Li, J.Z. Zhang, J. Phys. Chem. C 116 (2012) 17360–17368.
[25] L.F. Xu, Q.W. Chen, D.S. Xu, J. Phys. Chem. C 111 (2007) 11560–11565.
[26] J.H. Qiu, M. Guo, X.D. Wang, ACS Appl. Mater. Interfaces 3 (2011) 2358–2367.
[27] P.T. Hsieh, Y.C. Chen, K.S. Kao, C.M. Wang, Appl. Phys. A-Mater 90 (2008) 317–321.
[28] X.H. Lu, G.M. Wang, T. Zhai, M.H. Yu, S.L. Xie, Y.C. Ling, C.L. Liang, Y.X. Tong, Y. Li, Nano Lett. 12 (2012) 5376–5381.
[29] U. Ozgur, Y.I. Alivov, C. Liu, A. Teke, M.A. Reshchikov, S. Dogan, V. Avrutin, S.J. Cho, H. Morkoc, J. Appl. Phys. 98 (2005) 041301.
[30] W.M. Kim, Y.H. Kim, J.S. Kim, J. Jeong, Y.J. Baik, J.K. Park, K.S. Lee, T.Y. Seong, J. Phys. D Appl. Phys. 43 (2010) 295102.
[31] S.H. Lee, T.S. Lee, K.S. Lee, B. Cheong, Y.D. Kim, W.M. Kim, J. Phys. D Appl. Phys. 41 (2008) 095303.